Comparison of spectral models for disc truncation in the hard state of GX 339–4

Marta A. Dziełak[1] (mdzielak@camk.edu.pl), **Andrzej A. Zdziarski**[1] (aaz@camk.edu.pl), **Michał Szanecki**[1] (mitsza@camk.edu.pl), **Barbara De Marco**[1], **Andrzej Niedźwiecki**[2], **Alex Markowitz**[1,3]

1) Nicolaus Copernicus Astronomical Center, Polish Academy of Sciences, Bartycka 18, 00-716 Warszawa, Poland
2) Departament of Astrophysics, Łódź University, Pomorska 149/153, 90-236 Łódź, Poland
3) University of California, San Diego, Center for Astrophysics and Space Sciences, 9500 Gilman Dr, La Jolla, CA 92093-0424, USA

Abstract

We probe *models of disc truncation in the hard spectral state of an outburst of the X-ray transient GX 339-4*. We test a large number of different models of disc reflection and its relativistic broadening, using two independent sets of codes. We apply it to a Rossi X-ray Timing Explorer spectrum in the rising part of the hard state.
Our statistically best model has a physical thermal Comptonization primary continuum, requires the disc to be truncated at a radius larger than that of > 2 ISCO, and predicts a disc inclination in agreement with that of the binary. Our results has been published in Dziełak et. al., 2019, MNRAS, 485, 3845.

Introduction

The Shakura & Sunyaev (1973) model of accretion onto black holes predicts formation of a optically-thick disc extending down to the radius of the innermost stable circular orbit, R_{ISCO}. It explains well soft states of accreting systems. However, it cannot explain states with dominant hard X-ray radiation (Done, Gierliński & Kubota 2007). *That radiation has to be emitted by some hot plasma, which location remains not well understood.*

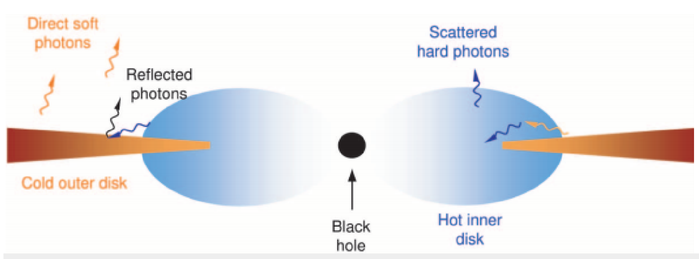

Figure 1: The one of the models of the accretion geometry in the hard state (Zdziarski, et. al. 2002).

Data

We have analysed the PCA (RXTE) observations of GX 339–4 (Fig. 2). We have combined spectra with similar flux and hardness. We have chosen the 2010/11 outburst, since it has the best coverage of the rising part of the hard state (Fig. 3).
We applied the correction to the effective area of García et al. (2014A), pcacorr.
Our results are based on a single spectrum (with 10^7 counts).

Discussion of results

Our main finding is that analysed spectra can be fitted with similar quality with models (with different physical assumptions) allowing significantly different disc truncation radii.

Still, all of the fitted models prefer the R_{in} much larger than R_{ISCO} at their best-fit values.

Model 0

That model keeps original assumptions from García et al. 2015 about two different iron abundances in inner and outer disc. This model requires the presence of a 7.2 keV absorption line and a high value of the Z_{fe}.

Single Fe abundance

We find $R_{in} >\sim 6\ R_{ISCO}$. The models no longer require the 7.2 keV absorption line and their fitted Fe abundances a relatively moderate, $Z_{Fe} >\sim 2$.

Model 6

Our statistically best model has a physical thermal-Comptonization primary continuum. The best fit value of the truncation radius is several tens of R_{ISCO}.
This model also has the best-fit inclination, in good agreement with the binary inclination (Heida et al. 2017).

Comptonization of reflected emission

For all of our models, we have also taken into account Comptonization of the reflected component. However, we have found this effect to be minor.

Reflector density

Using the model of García et al. (2016) with $n_e = 10^{19}$ cm^{-3} (#3 in Tab. 1), we have found an increase of both the truncation radius and the Fe abundance. The found increase of Z_{Fe} is surprising, given results of Tomsick et al. (2018) – who proposed high density as solution for high iron abundances.

Ionization of reflectors

Data allow for ionization parameters interchange. This effect is due to the relatively modest relativistic effects in the inner reflector. So our fits can not distinguish between inner and outer disc.

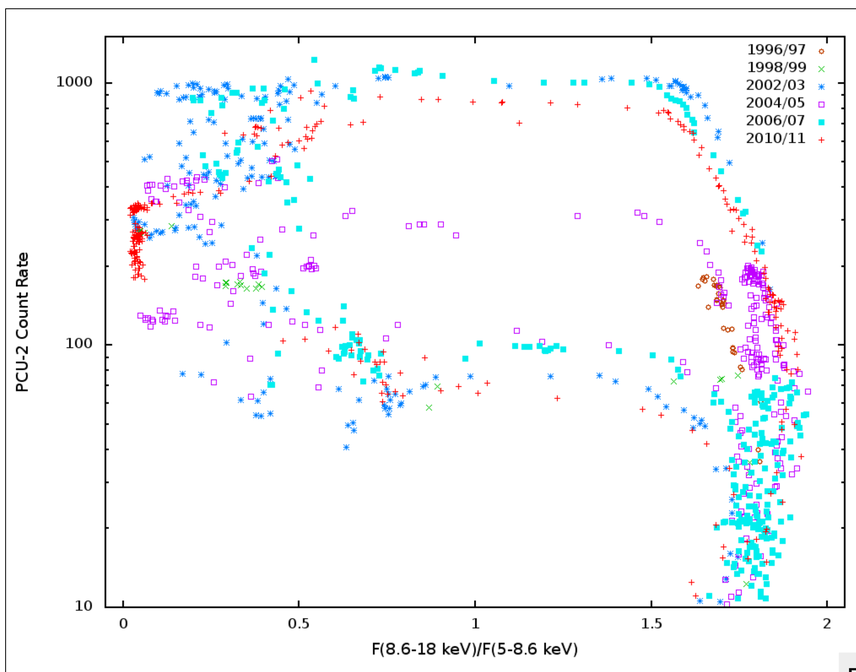

Figure 2: The count-rate vs. hardness diagram for 1107 PCA observations of GX 339–4 during its six major outbursts, identified by different colours. The hardness is defined as the energy flux ratio of the 8.6–18 to 5–8.6 keV bands.

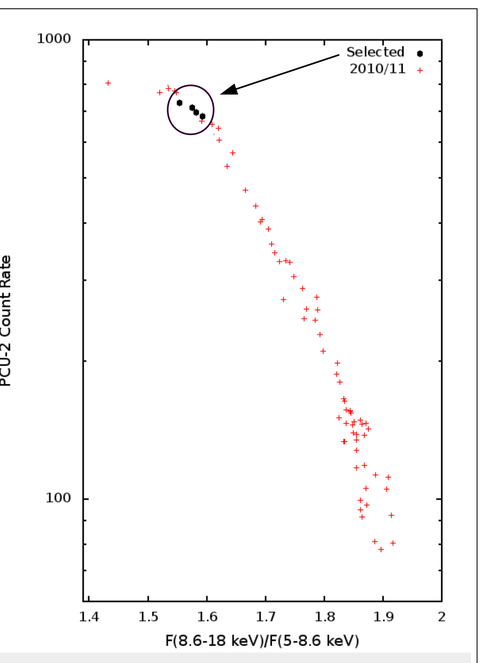

Figure 3: Subset of the data shown in Fig. 2 - the rise of the 2010/11 outburst. The black circles mark the observations forming the average spectrum fitted in this work.

Models

Using the X-Ray Spectral Fitting Package (xspec - Arnaud 1996) we probe models of disc truncation (reflection and relativistic broadening) using two independent sets of codes **relxill** (Garcıa, et al. 2014B) and **reflkerr** (Niedźwiecki, Szanecki & Zdziarski, 2019 - *https://users.camk.edu.pl/mitsza/reflkerr*).

The spectral fitting results for our models applied to average spectrum are presented in table 1.

Model 0: [relxill(free Z_{Fe})+xillver(Z_{Fe}=1)]gabs; ← two different iron abundances
Models 1 and 2: relxill + xillver; ← one iron abundance
Model 3: relxillD + xillverD; ← reflection from high density disc
Models 4 and 5: reflkerrExp + hreflectExp; ← incident e-folded power law
Model 6: reflkerr + hreflect. ← incident thermal Comptonization

		relxill			reflkerr		
Parameter/Model	0	1	2	3	4	5	6
$N_H/10^{21}$ cm^{-2}	$5.2^{+1.8}_{-1.2}$	$4.7^{+1.5}_{-0.3}$	$6.5^{+1.3}_{-1.7}$	$6.1^{+0.7}_{-0.6}$	$4.4^{+1.9}_{-0.4}$	$6.4^{+0.8}_{-1.1}$	$4.3^{+0.5}_{-0.3}$
Γ	$1.70^{+0.07}_{-0.04}$	$1.66^{+0.03}_{-0.04}$	$1.72^{+0.02}_{-0.03}$	$1.70^{+0.01}_{-0.05}$	$1.66^{+0.06}_{-0.02}$	$1.72^{+0.03}_{-0.01}$	–
y	–	–	–	–	–	–	$1.19^{+0.05}_{-0.08}$
E_{cut}/keV	200^{+130}_{-50}	250^{+50}_{-20}	300^{+80}_{-50}	300f	240^{+50}_{-50}	280^{+50}_{-20}	–
kT_e/1 keV	–	–	–	–	–	–	20^{+3}_{-2}
inner radii R_{in}/R_{ISCO}	11^{+10}_{-10}	19^{+33}_{-6}	$53^{+\infty}_{-26}$	$55^{+\infty}_{-34}$	15^{+31}_{-12}	$58^{+\infty}_{-28}$	$47^{+\infty}_{-45}$
iron abundance Z_{Fe}	$8.1^{+1.9}_{-5.5}$	$3.1^{+2.0}_{-0.3}$	$2.4^{+0.3}_{-0.2}$	$4.9^{+4.1}_{-0.9}$	$3.9^{+0.8}_{-1.4}$	$2.6^{+0.6}_{-0.4}$	$3.3^{+1.7}_{-1.0}$
i[°]	29^{+31}_{-29}	3^{+33}_{-3}	43^{+17}_{-23}	3^{+43}_{-3}	9^{+32}_{-9}	43^{+21}_{-19}	49^{+34}_{-26}
$\mathcal{R}$ (inner)	$0.059^{+0.001}_{-0.001}$	$0.170^{+0.004}_{-0.005}$	$0.144^{+0.004}_{-0.003}$	$0.059^{+0.033}_{-0.006}$	$0.25^{+0.04}_{-0.19}$	$0.35^{+0.06}_{-0.12}$	$0.42^{+0.36}_{-0.12}$
$\log_{10}\xi$ (inner)	$3.7^{+0.2}_{-0.5}$	$3.9^{+0.1}_{-0.1}$	$0.0^{+2.3}$	$3.7^{+0.1}_{-0.1}$	$3.9^{+0.1}_{-0.1}$	$1.7^{+0.7}_{-1.7}$	$3.9^{+0.1}_{-0.3}$
$\log_{10}\xi$ (outer)	0f	$1.7^{+0.5}_{-1.7}$	$3.8^{+0.2}_{-0.3}$	$0.7^{+1.0}_{-0.3}$	$2.0^{+0.3}_{-0.4}$	$3.7^{+0.1}_{-0.3}$	0f
$n_e/1\,\mathrm{cm}^{-3}$	10^{15}f	10^{15}f	10^{15}f	10^{19}f	10^{15}f	10^{15}f	10^{15}f
δ(gabs)	$0.011^{+0.011}_{-0.009}$	–	–	–	–	–	–
$kT_{bb}/1$ keV	–	–	–	–	–	–	$0.34^{+0.04}_{-0.09}$
χ^2_ν	65.6/61	68.7/61	68.3/61	72.4/62	69.1/61	69.2/61	62.1/61
p_i (AIC)	0.136	0.007	0.008	0.018	0.024	0.023	0.784
f_{sc}	$0^{+0.27}$	$0^{+0.29}$	$0^{+0.31}$	$0^{+0.12}$	$0^{+0.26}$	$0^{+0.79}$	$0.30^{+0.15}_{-0.30}$

Table 1: The spectral fitting results for our models applied to average spectrum.

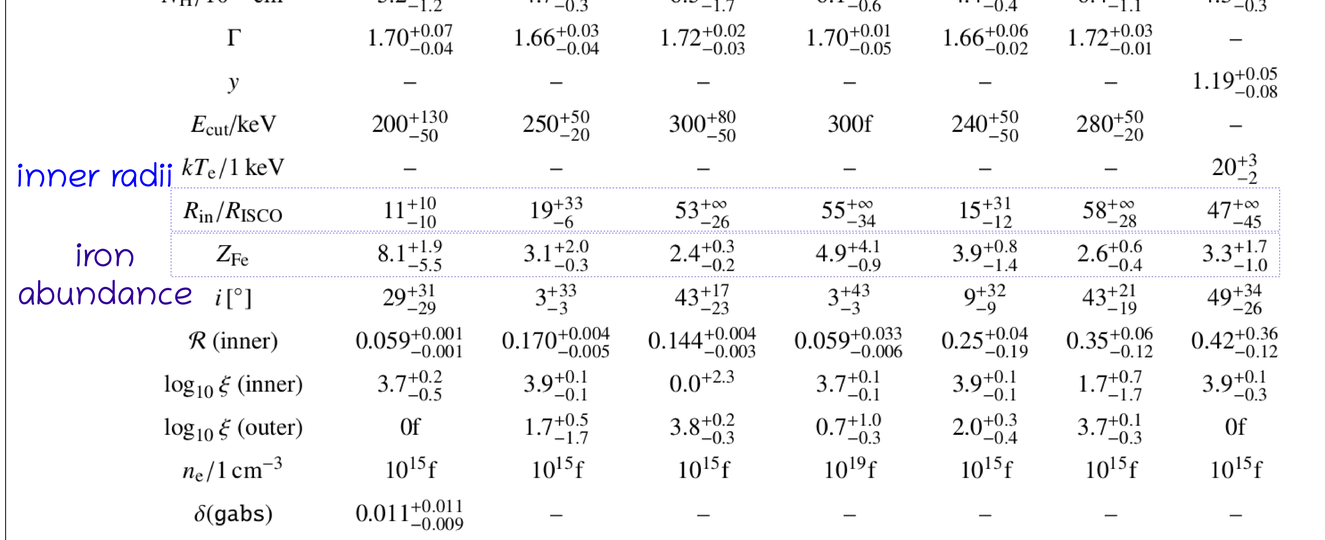

Figure 4:
Left - The histogram shows the unfolded spectrum (**model 6**): thermal Comptonization (dashed curve) and two reflectors, an inner highly ionized one (dot-dashed curve), and an outer weakly ionized one (triple dot-dashed curve). The solid curve gives the total model.
Right - The contributions to χ^2 of the model **#6**.